MAP2 is Hyperphosphorylated in Schizophrenia, Altering its Function

Grubisha, MJ[1]; Sun, X[1,2]; MacDonald, ML[1]; Garver, M[1]; Sun, Z[3]; DeGiosio, RA[1]; Lewis, DA[1]; Yates, NA[4,5]; Camacho, C[6]; Ding, Y[3]; Sweet, RA[1,7]

[1]Department of Psychiatry, Translational Neuroscience Program, University of Pittsburgh School of Medicine, 200 Lothrop Street, Pittsburgh, PA 15213, USA
[2] Tsinghua MD Program, Tsinghua Unviersity School of Medicine, Beijing, China
[3] Department of Biostatistics, University of Pittsburgh, Pittsburgh, PA 15260, USA
[4] Department of Cell Biology, University of Pittsburgh, 3500 Terrace Street, S362 Biomedical Science Tower (South) Pittsburgh, PA, 15261, United States
[5] Biomedical Mass Spectrometry Center, University of Pittsburgh, 5117 Centre Avenue, Pittsburgh, PA, 15213-1863, United States
[6] Department of Computational and Systems Biology, University of Pittsburgh, Pittsburgh, PA 15260, USA
[7] Department of Neurology, University of Pittsburgh School of Medicine, 200 Lothrop Street, Pittsburgh, PA 15213, USA
Corresponding Author: Robert A. Sweet, Translational Neuroscience Program, Biomedical Science Tower Room W-1653, 3811 O'Hara St Pittsburgh, PA 15213-2593. 412-624-0064, sweetra@upmc.edu

Abstract

Schizophrenia (Sz) is highly polygenic disorder, with common, rare, and structural variants each contributing only a small fraction of overall disease risk. Thus, there is a need to identify downstream points of convergence that can be targeted with therapeutics. Profound reduction of Microtubule-associated Protein 2 (MAP2) immunoreactivity (MAP2-IR) is present in ~60% of individuals with Sz, despite no change in MAP2 protein levels. MAP2 is phosphorylated downstream of multiple receptors and kinases identified as Sz risk genes, altering its immunoreactivity and function. Using an unbiased phosphoproteomics approach we quantified 18 MAP2 phosphopeptides, 9 of which were significantly altered in Sz subjects. Network analysis grouped MAP2 phosphorylations into 3 modules, each with a distinct relationship to dendritic spine loss, synaptic protein levels, and clinical function in Sz subjects. We then investigated the most hyperphosphorylated site in Sz, serine1782 (pS1782). Computational modeling predicted phosphorylation of S1782 reduces binding of MAP2 to microtubules, which was confirmed experimentally. Because only a limited number of MAP2 interacting proteins have been previously identified, we combined co-immunoprecipitation with mass spectrometry to characterize the MAP2 interactome in mouse brain. The MAP2 interactome was enriched for proteins comprising the ribosomal complex, including FMRP. This association was shown to be functional as overexpression of wildtype and phosphomimetic MAP2 reduced protein synthesis *in vitro*. These findings suggest a new conceptual framework for Sz - that a large proportion of individuals have a “MAP2opathy” - in which hyperphosphorylation of MAP2 mediates impairments of neuronal structure, synaptic protein synthesis, and function.

Introduction

Schizophrenia (Sz) is highly polygenic, with common, rare, and structural variants each contributing only a small fraction of overall disease risk[1]. Thus, there is a need to identify points of convergence, i.e. pathologies shared by large proportions of individuals with Sz, that can be therapeutically targeted to halt or reverse the synaptic[2] and functional deterioration[3,4] that occurs in affected individuals. Reduced Microtubule-Associated Protein 2 (MAP2) immunoreactivity (IR) has been reported in multiple cortical regions in Sz[5-10], leading one recent author to characterize it as a hallmark pathology in Sz[11]. Reduced MAP2-IR was not a consequence of common technical and clinical confounds of postmortem studies, suggesting it reflects an underlying pathogenic process [10,12].

In ~60% of individuals with Sz, the reduction in MAP2-IR is profound [10,12,13]. Even in these cases in which MAP2-IR is markedly reduced, it is not due to loss of MAP2 protein itself[10], and thus must reflect reduced detectability of MAP2 by antibody. Phosphorylation of MAP2 is known to alter its structure, function, and immunoreactivity (IR)[14], and to be regulated downstream of multiple genes now established by unbiased methods as Sz risk genes[15-23]. As the predominant regulator of the dendritic microtubule cytoskeleton, as well as a noted coordinator between microtubule and actin dynamics[24], alterations to MAP2 function could explain a variety of abnormalities in dendritic structure which have been observed across multiple cortical regions in Sz. Many groups have reported reduced pyramidal neuron somal volume[25-28], dendritic arborization[29-33], dendritic spine density and number[10,31,32,34-36], to be present in multiple cortical regions in Sz. These include our studies of primary auditory cortex[10,36,37].

Thus, we hypothesized that MAP2 phosphorylation would be altered in Sz and alter MAP2 functions, providing a potential hub for pathogenesis. To evaluate this, we undertook a phosphoproteomic analysis of MAP2 in primary auditory cortex of Sz and control subjects. We identified 9 phosphopeptides whose levels were significantly altered in Sz. These phosphopeptides grouped into 3 modules using network analysis, each with a distinct relationship to clinicopathologic correlates of disease. We designed a series of experiments to further investigate the most altered phosphorylation site, serine 1782 (pS1782), finding that phosphorylation at this site reduces microtuble binding. Finally, using MAP2 co-IP coupled with mass spectrometry, we found that the MAP2 interactome was enriched for ribosomal proteins, suggesting that MAP2 may play a role in translational regulation. This association was shown to be functional as overexpression of wildtype and phosphomimetic (pS1782) MAP2 reduced protein synthesis *in vitro*.

Methods

Preparation of expression constructs

IRES-MAP2c-EGFP plasmids containing cDNAs encoding human MAP2c (NM_031845) was purchased from GeneCopoeiaTM (Cat#: CS-E2438-M61-01). Although MAP2c is a shorter isoform, we use the amino acid numbering designated by full-length MAP2 throughout unless specifically referring to an experiment using the MAP2c plasmid (i.e. S426 in MAP2c corresponds to S1782 using numbering based on MAP2b). MAP2c phosphomimetic mutant S426E was generated using the QuikChange Lightning site-directed mutagenesis kit (Agilent Technologies) and mutagenized primers (Table 1). Plasmids were purified using the EndoFree Plasmid Maxi Kit (Qiagen). Presence of the mutation at the desired site without additional off-target effects was evaluated by Sanger sequencing (Table 1).

Cell culture and transfection

HEK cells were grown in RPMI-1640 containing 5% fetal bovine serum (Cellgro, Manassas, VA) without antibiotics. They were grown in a humidified chamber at 37 degrees Celsius with 5% CO_2. They were passaged appropriately during linear growth phase to maintain sub-confluent culture. For transfections they were seeded at $1.5x10^5$ cells/well into 12-well culture-treated plates. They were serum starved for 16h overnight, then replenished with complete media at the time of transfection the following morning.

Transfection

All transfections were performed using Lipofectamine LTX with Plus reagent (ThermoFisher Scientific, Grand Island, NY) in the absence of antibiotics. Media was changed 16h after transfection.

Western Blotting

Cell-free protein lysates were obtained from cells using radioimmune precipitation assay buffer (10 mM Tris-HCl, pH 8.0, 1 mM EDTA, pH 8.0, 0.5 mM EGTA, 140 mM NaCl, 1% Triton X-100, 0.1% sodium deoxycholate, 0.1% SDS), and total protein levels were quantified using the Lowry protein assay (Bio-Rad). 15 µg of total protein was loaded per well. Samples were electrophoresed on a NuPage Bis-Tris 4-12% gradient polyacrylamide gel (ThermoFisher Scientific) and transferred to a PVDF membrane (Millipore, Danvers, MA) at 100V for 1h. Membranes were blocked in Licor Blocking buffer (Odyssey, Lincoln, NE) for 1h at room temperature and primary antibody was added and incubated overnight at 4 degrees Celsius. The following primary antibodies were used in this study: mouse anti-MAP2 (HM-2, Abcam, 1:1000), rabbit anti-β tubulin (Abcam, 1:10,000), and mouse anti-puromycin (12D10, Millipore Sigma, 1: 25,000). Membranes were washed 5x5min in TBS containing 0.1% Tween and incubated with fluorescent-conjugated secondary antibodies (1:10,000) for 1h at room temperature. Five more washes were performed and membranes were imaged using the Odyssey Licor System. Densitometric analyses were performed using MCID Core Analysis software (UK).

Table 1. Primer sequences

TARGET	FORWARD (5'-3')	REVERSE (5'-3')
S1782E mutagenesis	CCACGCTGGATCTGCCTGGTTCCTGT GTAATGATCTCAGCC	N/A
MAP2c sanger sequencing	Primer 1: GCGGTAGGCGTGTACGGT Primer 2: TTCACGCACACCAGGCACT Primer3: TAGACCTAAGCCATGTGACAT	Primer 1: AGCAGTCCCCAAGTCAGT Primer 2: AGTGCCTGGTGTGCGTGAA Primer3: GAGAAGGAGGCAGATTAGCTG

Co-immunoprecipitation

For co-immunoprecipitation (Co-IP) from 4-week old mouse brain tissue, mice were sacrificed by lethal CO2 followed by rapid decapitation. Whole mouse brains were then extracted, snap frozen and stored at -80 °C until use. Frozen brain tissue was manually homogenized in ice-cold 0.5% NP-40 IP lysis buffer with RNAse (100uL per 1mL of lysis buffer) by micro-pestle and passing through 23G needle multiple times. The lysate was then incubated on ice for 10 min followed by centrifugation at 14,000g for 20 min at 4 °C to remove the insoluble fraction. The supernatant was centrifuged again at 12,000g for 10 min at 4 °C. The supernatant was transferred to a new tube, 50µl of which was saved as input, and the rest of the supernatant was precleared by incubation with 1mg 1xPBS pre-washed Dynabeads (Thermo Fisher Scientific) on a rotator at 4°C for 1h. To prepare the antibody-coupled beads, HM-2 antibody (Abcam, Cambridge, MA, USA) was incubated together with washed Dynabeads (8µg antibody per mg beads used) in 1x PBS buffer with 0.1M citrate (pH 3.1) on a rotator at 4°C overnight. The precleared supernatant was incubated with antibody-coupled beads on a rotator at 4°C overnight. Controls were generated using washed beads not coupled to antibody. Following overnight incubation, the supernatant was collected and saved in a new tube. The Co-IP beads were washed three times in ice-cold 1xPBS buffer by gentle pipetting and directly boiled in 60 µl 1x SDS sample buffer (30 mM Tris-HCl, pH 7.4, 1% SDS, 12.5% glycerol, 2.5% β-mercaptoethanol, 0.05% Orange G) at 95 °C for 5 min to elute protein complexes from the beads.

In-gel trypsin digestion

Immunoprecipitated samples were shortly separated (1cm) by SDS-PAGE and stained with SimplyBlue™ SafeStain (Thermo Fisher Scientific). The stained gel regions were excised and in-gel trypsin digested as previously described [38]. In brief, the excised gel bands were washed with HPLC water and destained with 50% acetonitrile (ACN)/25mM ammonium bicarbonate until no visible staining. Gel pieces were dehydrated with 100% ACN, reduced with 10mM dithiothreitol (DTT) at 56°C for 1 hour, followed by alkylation with 55mM iodoacetamide (IAA) at room temperature for 45min in the dark. Gel pieces were then again dehydrated with 100% ACN to remove excess DTT and IAA, and rehydrated with 20ng/µl trypsin/25mM ammonium bicarbonate and digested overnight at 37°C. The resulting tryptic peptides were desalted with Pierce C18 Spin Columns, speed-vac dried and resuspended in 18µL 0.1% formic acid. A pooled instrument control (PIC) was made by taking 3µL from each of the samples.

Human Subjects and Animals

Tissue was obtained from postmortem brains recovered during autopsies conducted at the Allegheny County Medical Examiner's Office, Pittsburgh, PA, following informed consent from the next of kin. All procedures were approved by the University of Pittsburgh Committee for the Oversight of Research and Clinical Trials Involving the Dead and the Institutional Review Board for Biomedical Research as previously described[39,40]. An independent committee of experienced clinicians made consensus Diagnostic and Statistical Manual of Mental Disorders, Fourth Edition diagnoses, or absence thereof, for each subject using medical records, structured interviews with surviving relatives, and, when available, toxicology reports. A cohort comprising 16 individuals with a consensus diagnosis of schizophrenia (Sz) and 16 matched non-psychiatric control (NPC) subjects was generated (Table S1). The Sz subjects were further divided by MAP2 immunoreactivity (MAP2-IR) as either low (MAP2-IR_{LOW}) or normal (MAP2-IR_{NL})[41]. Tissue slabs containing the superior temporal gyrus with Heschl's Gyrus (HG) located medial to the planum temporal were identified, and the superior temporal gyrus (STG) removed as single block. The samples were then distributed in a block design for preparation and analysis to evenly distribute SZ and control samples and blind the experimenters during sample preparation, analysis, and peak integration. Gray matter was collected from HG by taking 40 µm sections and frozen at -80 °C[42].

In order to account for the effects of chronic antipsychotic drug administration, a cohort of 18 male rhesus monkeys, n = 6 per group, were administered therapeutically relevant doses of haloperidol, olanzapine, or vehicle. The tissue utilized here has been extensively described elsewhere[43,44]. Briefly, tissue slabs containing the superior temporal gyrus were removed in a single block and 20 mg of gray matter was harvested as described above. A mouse model of postmortem interval (PMI) was generated using wildtype C57/Bl6J mice purchased from Jackson Laboratories (Bar Harbor, ME, USA). Adult mice, n= 2 per timepoint (0, 6, 12, 18, 24 hrs), were sacrificed by CO_2 asphyxiation followed by cervical dislocation. The carcasses were incubated at room temperature for 2/3 the PMI duration and then placed at 4°C for the final 1/3. The brain was then removed from the skull, the cerebellum discarded, and the hemispheres separated (giving n = 4 hemispheres/time point), flash frozen in isopentane on dry ice, and stored at -80°C until use.

Mass Spectrometry

Sample Preparation – Phosphopeptide enrichment

Gray matter from primary auditory cortex was harvested as previously described[45]. Protein quantification was determined by using a micro bicinchoninic acid assay. The samples were processed across multiple runs, using a balanced block design to evenly distribute schizophrenia and control subjects. Each run was processed identically. To account for biological and experimental variation, pooled controls were included in the designed and interspersed throughout. 500µg of protein from each gray matter homogenate sample were in-solution

digested overnight at 37C with trypsin at a ratio of 1:50 (ug trypsin: ug total protein). Samples were then desalted using Oasis cartridges. Phosphorylated peptides were enriched using Titanium Dioxide Phosphoenrichment. To perform the titanium dioxide phosphoenrichment, ToptTips TiO_2 + ZrO_2 (Glygen Corporation, Columbia, MD, USA)) were washed three times with loading buffer (19% lactic acid, 80% ACN, 1% formic acid) and centrifuged 30 sec x 0.5g. Beads were suspended to 50% slurry with the loading buffer and 20µL of bead slurry was added to each sample. The sample + bead mixtures were rotated for 1 hour. Samples were spun 30sec x 0.5g and supernatant was removed. 1 mL of the loading buffer was added to each sample, and rotated for 5 minutes. Samples were centrifuged and supernatant removed. Sample was suspended in 200µL washing buffer (80% ACN, 5%TFA) and centrifuged through a C18 Stage tip. C18 stage tip was subsequently washed x4 with washing buffer. Phosphopeptides were eluted with 50µL elution buffer (450µL Ammonium Hydroxide (28%) in 4.5 mL DI H_20 pH 11) 2 times. Elution buffer was evaporated and samples re-suspended in 20µL 98% buffer A (0.1% formic acid/DI H_20) 2% buffer B (0.1% formic acid/ACN). Samples were then analyzed by LC-MS/MS.

Liquid Chromatography Tandem Mass Spectrometry: Phosphopeptides

Phosphopeptide enrichments were analyzed by reversed phase nanoflow liquid chromatography tandem mass spectrometry (nLC-MS/MS) using a nanoACQUITY (Waters Corporation, Milford, MA, USA) coupled to an Orbitrap XL hybrid ion trap mass spectrometer (ThermoFisher Scientific, Waltham, MA, USA). For each nLC-MS/MS analysis, 1 µL of peptides was injected onto a C18 column (PicoChip™ 25 cm column packed with Reprosil C18 1.9 µm 120Å chromatography media with a 75 µm ID column and 15 µm tip; New Objective, Inc., Woburn, MA, USA) and eluted into the mass spectrometer with a 60 min linear gradient of 5-35% ACN/0.1% FA at a 300 nL/min. A data-dependent top 4 method was used with full scan resolution set at 60,000. Ions were isolated for MS/MS analysis with a 2.0 Da window. Dynamic exclusion was enabled to minimize the redundant selection of peptides previously selected for MS/MS. Ion chromatograms of 10 selected peptides were extracted using Skyline software[46] and used to monitor during the instrumental analysis to ensure robust instrument performance.

LC--MS/MS – MAP2 co-IP

Extracted tryptic peptides were analyzed by nano reversed-phase liquid chromatography tandem mass spectrometry (nLC-MS/MS) using a nanoACQUITY (Waters Corporation, Milford, MA, USA) online coupled with an Orbitrap Velos Pro hybrid ion trap mass spectrometer (Thermo Fisher Scientific). For each LC-MS/MS analysis, 1 µL of peptides was injected onto a C18 column (PicoChip™ 25 cm column packed with Reprosil C18 3 µm 120Å chromatography media with a 75 µm ID column and 15 µm tip; New Objective, Inc., Woburn, MA, USA) and then eluted off into the mass spectrometer with a 66 min linear gradient of 2-35% ACN/0.1% FA at a 300 nL/min. A data-dependent top 13 method was used with full scan resolution set at 60,000. Ions were isolated for MS/MS analysis with a 2.0 Da window. Dynamic exclusion and chromatograms from 20 selected peptides were utilized as described above.

Data analysis

MS/MS spectra from both the phosphopeptide and MAP2 co-IP experiments were searched using MASCOT search engine (Version 2.4.0, Matrix Science Ltd, Boston, MA, USA) against the UniProt human and mouse proteome databases. The following modifications were used: static modification of cysteine (carboxyamidomethylation, +57.05 Da), variable modification of methionine (oxidation, +15.99Da). The mass tolerance was set at 20ppm for the precursor ions and 0.8 Da for the fragment ions. Peptide identifications were filtered using PeptideProphet™ and ProteinProphet® algorithms with a protein threshold cutoff of 99% and peptide threshold cutoff of 90% implemented in Scaffold™ (v4.7.5; Proteome Software, Portland, Oregon, USA). Skyline MS1 filtering[47] was used for batched integration of ion chromatograms of all identified peptides. MS2 spectra for MAP2 were manual sequenced to confirm the phosphopeptide-spectra match and confidence of phospho-site assignment.

Microtubule-binding (MTB) assay

Transfected HEK293 cells were harvested 48 h post transfection with ice-cold microtubule-binding buffer (80 mM Pipes, 5 mM MgCl2, 0.5 mM EGTA) supplemented with 1% Triton X-100 and protease/phosphatase inhibitors (Millipore, Burlington, MA, USA; and Sigma, St. Louis, MO, USA, respectively) and lysed by vortex and passing through a 26G needle multiple times. Protein lysates were first centrifuged at 17,000g for 10 min at 4 °C to remove insoluble cell debris, after which the supernatant was collected and further pre-cleared by ultracentrifugation at 100,000 g for 40 min at 4°C. *In vitro* microtubule-binding assay was performed using the microtubule-binding protein spin down assay kit (Cytoskeleton, Denver, CO, USA) according to the manufacturer's instructions. Briefly, microtubules were freshly polymerized and kept at room temperature prior to use. For each microtubule binding reaction, 20µl freshly prepared microtubules were incubated with a series of volumes (10 µl /20 µl /30µl) of pre-cleared cell lysate for 30 min at room temperature. Pre-cleared cell lysate alone in incubation reaction was included as negative control. Moreover, MAP fraction (contains 60% MAP2 at 280 kDa and 40% tau proteins at 40-70 kDa) and BSA, each incubated with the polymerized microtubules, served as a technical positive and negative control, respectively. Reaction solution was then placed on top of 100 µl taxol supplemented Cushion buffer (80mM PIPES pH 7.0, 1 mM MgCl2, 1 mM EGTA, 60% Glycerol) and centrifuged at 100,000 g for 40 min at room temperature. The pellets containing microtubules and their binding proteins were resuspended in 1x SDS sample buffer as described above. Supernatant and pellet samples were analyzed by SDS-PAGE and Western blot.

MD simulation

The molecular dynamic (MD) systems were built using cubic TIP3P water box with 12 Å buffer around the solute following the general procedure of protein system building in CHARMM-GUI. Cl- and Na+ ions were added to the solvent to neutralize the charge of the systems. All MD simulations were performed using NAMD and CHARMM C36m FF (optimized for disordered proteins). Secondary structure analysis of MD simulation trajectories were carried out using Timeline Plugin available within VMDv1.9.2. Initially all systems were minimized twice and then equilibrated them before beginning production runs. In the first minimization solute, atoms were held fixed through 500 steps of steepest descent and 500 steps of conjugate gradient minimization. In the second minimization, only the solute backbone atoms were restrained through 2000 steps of steepest descent and 3000 steps of conjugate gradient. After minimization, system temperature was raised to 300 K over the course of a 100 ps constant volume simulation during which the solute is fixed with weak (10.0 kcal/mol) restraints. For the production run, the 500 ns simulations was held at constant temperature 300 K and under constant pressure of 1 bar without any restraints used during equilibration step. For this, Langevin dynamics was used to maintain constant temperature with a Langevin coupling coefficient of 1 ps–1, and a Nosé-Hoover Langevin piston was used to maintain constant pressure with a piston period of 50 fs and a piston decay time of 25 fs while keeping barostating isotropic. A 2-fs timestep was used for integration together with the SHAKE algorithm where all covalent bonds between hydrogen and the heavy atom are constrained. The van der Waals interactions were smoothly switched off at 10 – 12 Å by a force-switching function while the long-range electrostatic interactions were calculated using the particle-mesh Ewald method.

Surface sensing of translation (SUnSET) Assay

Surface sensing of translation (SUnSET) assay was performed as previously described[48] with minor modifications: HEK293 cells were incubated with 10 µg/ml of puromycin in cell culture media for 1 h before harvest. As a negative control, cells were pretreated with 10 µL of cycloheximide (CHX) to inhibit protein synthesis for 1h before puromycin treatment. No puromycin incorporation was detected under these conditions (data not shown). Levels of newly synthesized proteins incorporating puromycin were measured using western blots as described above.

Statistical analysis

Student's t-test on log2 transformed peptide peak area was used for the statistical inference to select Map2 interacting partners. A peptide was considered differentially ID'd if the q-value was <.1 and a positive Map2 CoIP:Control ratio value.

Statistical analyses for the MTB and puromycin incorporation assays were performed in SPSS software with One-way ANOVA and Bonferroni post-hoc test to determine statistically significant differences for all the comparisons. All statistical tests were two-sided with α= 0.05. Data are displayed ± standard error of mean (SEM).

Differential expression analysis on phosphorylation

ANCOVA was performed to detect the difference across Sz with MAP2-IR$_{LOW}$, Sz with MAP2-IR$_{NL}$, and NPC samples in 18 MAP2 phosphopetides. PMI and assay run were adjusted as covariates. Fold changes, p-values, and q-values between each Sz group and control samples are presented (Table 2).

We also analyzed the association between MAP2 phosphopetides and each demographical or clinical variable using a similar ANCOVA model to detect potential confounders, where diagnosis, PMI and assay run were adjusted. P-values and q-values for each variable are presented (Table S2).

Network Analysis: Weighted Gene Co-expression Network Analysis (WGCNA)[49] was used to investigate the pattern of co-regulated phosphopeptide expression in all samples. Topological overlap matrix will be used to identify modules with clustered phosphopetides. The three identified networks were visualized using Cytoscape. To quantitate the representation of expression levels in each module, we calculated the first principal component of modules given by WGCNA, referred to as the module-specific eigenpeptide. Linear regression models were fitted to model the correlation between each module-specific eigenpeptide and dendritic spine density, synaptic protein levels, and socioeconomic status (SES), with diagnosis (Sz or control) adjusted.

Results

MAP2 is hyperphosphorylated in auditory cortex in Sz

We conducted an unbiased proteomic survey of MAP2 phosphorylation in primary auditory cortex (A1) obtained from Sz subjects with either profoundly reduced MAP2-IR in A1 (MAP2-IR$_{LOW}$, N=11)[10] or normal MAP2-IR (MAP2-IR$_{NL}$, N=5), and from non-psychiatric control (NPC, N=16) subjects (see Table S1 for subject characteristics). We identified 18 unique MAP2 phosphopeptides in our samples, confirmed by manual sequencing of MS2 spectra, 8 of which were significantly altered (q<0.05) in MAP2-IR$_{LOW}$ Sz subjects relative to NPC subjects. The most altered phosphopeptide, VDHGAEIITQS[+80]PGR, containing a single phosphorylation at serine 1782 (pS1782, numbering per the canonical MAP2b isoform, Uniprot identifier: P11137-1), was increased up to nearly 9-fold relative to NPC subjects (Fig 1B upper panel, Table 2). In MAP2-IR$_{NL}$ Sz subjects, changes in phosphopeptide levels were mostly attenuated, although in the combined Sz group a total of 9 phosphopeptides now reached significance (Table 2). Elevated levels of MAP2 phosphopeptides were largely unassociated with potential tissue and clinical confounds (Table S2) with two notable exceptions. First, levels of VDHGAEIITQS[+80]PGR were significantly lower in Sz subjects taking antipsychotics at time of death than in those subjects off antipsychotics, raising the possibility that antipsychotic treatment could act, in part, through effects on phosphorylation of S1782. However, this effects was not recapitulated by a monkey model of long-term antipsychotic exposure, nor did this model induce elevations of any phosphopeptides found to be elevated in MAP2-IR$_{LOW}$ Sz (Fig 1A, lower panel). Second, phosphopeptide abundance may be subject to substantial alterations from postmortem interval (PMI). Thus, we further evaluated this potential confound in 2 ways. We first tested the effect of PMI on phosphopeptide abundance in our subjects, finding no significant associations (all q>0.1, Table S2). Second, we surveyed MAP2 phosphopeptide abundance in a mouse model of increasing PMI. We detected 9 MAP2 phosphopeptides in this model. Fig 1B shows the detected MAP2 phosphopeptides, 8 of

which demonstrate stable or linear changes over time (and thus readily accounted for by PMI matching in our subjects). Of note, one peptide (RL*S[+80]*NVS*S[+80]*SG*S[+80]*INLLESPQLATLAEDVTAALAK) had a nonlinear decay, so although included in network analysis (see below) it was not considered a candidate for further study.

We next applied Weighted Gene Co-Expression Network Analysis (WGCNA)[49] to the MAP2 phosphopeptide data from the Sz and NPC subjects. MAP2 phosphopeptides clustered into three modules (Fig 2A-C). We then used these three modules to compute eigenpeptide values for all subjects and tested these values for their associations with known pathological features of disease, namely decreased dendritic spine density and decreased synaptic protein levels, both of which had been previously measured in these subjects[40,50]. Furthermore, socioeconomic status (SES) was included as a proxy measure for functional impairment in Sz[51], thus we also tested the eigenpeptide values for their association with subject SES (Table 3). Levels of phosphorylation of blue module sites, which include pS1782, are associated with lower spine density, reduced synaptic protein levels, and poorer outcomes (lower SES). Figure 2D shows the negative correlation between dendritic spine density and pS1782 levels. In contrast, increasing phosphorylation of brown module sites, which are only present in the MAP2a and MAP2b isoforms, are correlated with better phenotypic outcomes. Turquoise module phosphopeptides show little relationship to the measured phenotypes.

Phosphorylation of MAP2 at S1782 alters its predicted structure and reduces microtubule binding

The phosphopeptide with the most elevated levels in MAP2-IR$_{LOW}$ Sz was VDHGAEIITQS$^{[P]}$PGR, phosphorylated at S1782. This peptide belongs to the blue module, which includes negative correlations with dendritic spine density and synaptic protein levels. Furthermore, S1782 is conserved in the MAP2 homolog microtubule-associated protein tau (MAPT), as S396 (numbering by common convention as per Isoform Tau-F, Uniprot identifier: P10636-8), which when phosphorylated confers synaptic pathology[52-55]. We used all atom Molecular Dynamics simulations (MDS) to predict potential effects of pS1782 on MAP2 structure. Like its homolog MAPT, structure of the intrinsically disordered MAP2 is difficult to characterize. Because MAP2 and MAPT share high sequence homology, to validate our model we first checked for consistency with available information in both MAP2[56,57] and MAPT[58,59]. For this validation we relied on the known effect of phosphorylation at T231 in MAPT (homologous to T1649 in MAP2). For example, our model of pT1649 MAP2 revealed a salt bridge interaction between pT1649 and R1648 and helical propensity for the region ^{299}ATPKQLRLR^{307}, both of which predictions recapitulated prior observations for the corresponding residues in MAPTau (data not shown)[60-63]. We then examined phosphorylation at S1782 by simulating a region of MAP2 containing residues 1718 to 1827 (covering the C-terminal domain). Our models indicated two structural changes upon phosphorylation of S1782: (a) an antiparallel β hairpin structure observed in wild-type (WT) MAP2 opened up to create a solvent-exposed extended β structural conformation between A1776 and S1782; and (b) pS1782 induced a solvent-exposed extended β structural conformation between residues V1755 and A1770, whereas helical structural propensity was present in WT MAP2 (Fig. 3). The homologous residues K369 to A384 in Tau are part of the C-terminal (residues K369 to S400) that flank the MT binding region and have been proposed for positioning Tau on the MT surface allowing MT binding[64-66]. More recently, NMR showed that pS396 MAPT had weaker tubulin affinity than the wild type Tau peptide with signal attenuation centered around residues H374, F378, H388 and Y394[67]. Based on these data, we predicted that MAP2 pS1782 decreases MT binding.

To empirically evaluate these predictions, HEK cells, which lack endogenous MAP2, were transfected with plasmid containing either wildtype MAP2c (Uniprot identifier: P11137-2) or MAP2c with the phosphomimetic mutation S426E, homologous to S1782 in full length MAP2b (see Methods for plasmid construct information), and a microtubule (MT) binding assay was performed. The results of the MT binding assay are shown in Figure 3B&C and confirm the computationally-predicted reduction of MT binding by S426E MAP2c.

MAP2 interacts with ribosomal complexes and inhibits protein synthesis

MAP2 binding to MTs can sequester MAP2 and its binding partners[68]. Conversely, reduced MAP2 binding to MTs increases the availability of MAP2 to associate with alternate interaction partners[69], creating what in essence is a gain of function of these latter effects. We therefore sought to use an unbiased proteomic screen of the MAP2 interactome to identify additional potential interaction partners. Co-IP of MAP2 from RNAse-treated whole brain homogenate from C57Bl6J mice (N=3 mice, 6 hemispheres total as biological samples) resulted in identification of 590 proteins that were potential interactors of MAP2 ($q<.05$) for MAP2 IP compared to no

antibody control (Fig 4A-C ,Table S3). Our unbiased approach highlighted an interaction previously observed in neurons, although underappreciated, between MAP2 and ribosomal complexes[70]. Functional annotation analysis[71] of these proteins revealed enrichment for terms related to translation (e.g. GO:0006412~translation, corrected $p=1.4E^{-30}$, N=71 proteins, 44 of which are ribosomal subunits). Table S4 shows the 3 highest scored GO categories within the top 8 functional annotation clusters.

Based on the above association of MAP2 with ribosomal complexes, we next hypothesized that MAP2 may play a role in translational regulation. To test this, we measured incorporation of puromycin, an indicator of new protein synthesis[48]. Expression of both WT or S426E MAP2c in HEK293 cells suppressed new protein synthesis compared to empty vector control, though the magnitude of this effect was slightly greater in S426E (Fig 4D&E).

Discussion

MAP2 is the predominant dendritic MAP in the brain, where its modification by phosphorylation downstream of glutamate signaling[17] has been postulated to be a requisite step linking experience to structural plasticity of dendrites[72]. We implemented a phosphoproteomics approach to evaluate this post-translational modification of MAP2 in Sz subjects in comparison to NPC subjects. We identified 18 unique MAP2 phosphopeptides in our samples, 9 of which were significantly altered in Sz compared to NPC subjects. Abnormally phosphorylated peptides were located predominantly in the Proline Rich and C-terminal domains which flank the MT Binding domain and are present in all isoforms. The most altered site was pS1782, which was found to be increased nearly 9-fold in Sz subjects compared to NPC subjects. We carefully considered potential confounds (e.g. PMI, pH, tissue storage time, age, race, sex, antipsychotic treatment, substance use, tobacco use) in our human subjects, none of which accounted for the elevation in phosphopeptides in Sz. Instead, a module of co-occurring phosphopeptides including pS1782, correlated with increasing severity of structural, proteomic, and functional measures in our subjects, suggesting the possibility that some or all of these co-occurring phosphorylations may causally contribute to the pathogenesis of Sz. To evaluate potentially causality, we chose the most elevated phosphopeptide, containing pS1782, as a candidate for further study.

Prior studies have shown that phosphorylation of MAP2 within its MT binding domain and proline rich domains reduce MT binding by MAP2,[14] and thus alter their dynamics.[73] Given the proximity of S1782 to the microtubule binding domain of MAP2, we utilized computational modeling to predict the effects of this modification on structure. We now show that phosphorylation of S1782 in the c-terminal domain of MAP2 can act similarly to phosphorylation at the homologous S396 in MAPT, which (in combination with pS404) is primarily responsible for MAPT dissociating from MTs.[74] Subsequent *in vitro* studies confirmed this finding, demonstrating reduced MT-binding in an S426 (MAP2c) phosphomimetic construct.

Our computational models similarly identified a set of β-strands induced by S1782 phosphorylation between K368-V372 and A420-Q425, a more open configuration that provides more conformational combinations required for protein-protein interaction and thus the potential for an additional gain of pathologic functions. Specifically, we hypothesized that the reduced MT-binding affinity caused by (pseudo)phosphorylation of S1782 would lead to increased MT-unbound MAP2 levels. Previous work has shown binding by some proteins to only MT-unbound MAP2[75], suggesting that a careful balance between MT-bound and -unbound MAP2 may be necessary for proper cellular functioning. Hence this increase, in combination with new protein interactions enabled by the conformational changes, provides a means by which phosphorylation of MAP2 may yield additional pathological gains of function in schizophrenia. To determine the nature of these additional functions, we combined immuno-enrichment with LC-MS/MS to characterize the MAP2 interactome. These studies revealed that the MAP2 interactome was enriched for interactions with ribosome and RNA-binding proteins forming the translational machinery (Table S3). This finding is unlikely to be artifactual, as we eliminated the possibility of residual RNA binding through RNAse treatment prior to the co-IP. This finding suggests a novel role for MAP2 in regulation of protein translation. To determine the nature of this alternative function of MAP2 we used puromycin incorporation to measure protein synthesis. We found that overexpression of MAP2c suppresses protein translation, an effect which is slightly, though non-signficantly, enhanced by pseudophosphorylation at S426 (MAP2c). Taken together, these findings are the first to suggest that MAP2 may have an additional function in regulating protein translation. Although there was a non-signficant difference in this function between WT and S426E MAP2c, it warrants further consideration in future studies that

phosphorylation at other sites, alone or in combination, may alter this novel function of MAP2.

Nevertheless, the association of MAP2 with the protein translation machinery, and more importantly our novel demonstration that overexpression of WT or S426E MAP2 inhibits protein synthesis, provide a potential mechanism by which MAP2 may mediate synaptic plasticity. A number of mRNAs are translated explicitly in dendrites after synaptic stimulation to provide rapid regulation of local protein levels in support of structural and functional plasticity.[76] Specific mRNAs are maintained in a translationally repressed state before being transported to dendrites.[77] This translational repression is mediated, to a large extent, by Fragile X Mental Retardation Protein (FMRP), encoded by the FMR1 gene, and related protein family members. Altered FMRP levels,[78] and genetic variants in targets of FMRP,[21] have been previously associated with schizophrenia. Our data suggest this might involve dysfunction of MAP2 which is a known target of FMRP[79] and which was associated with FMRP and related proteins in our co-IP experiments (Table S3). In fact, FMRP maps into the most enriched cluster, Intracellular ribonucleoprotein complex (GO:1990904), of these proteins (Table S4). The possibility that repression of synaptic protein synthesis by MAP2 has a role in the pathogenesis of Sz was further supported by our observation of the correlation of the blue module, containing pS1782, with reduced levels of multiple synaptic proteins in synaptosomes of subjects with Sz.

In summary, we identified a novel pathology of Sz, hyperphosphorylation of multiple peptides within MAP2. We further demonstrated that at least one of these phosphorylations, pS1782, impairs MAP2 MT binding and inhibits new protein synthesis, functions critical for dendritic plasticity. These findings provide a new conceptual framework for schizophrenia as a “MAP2opathy”. That is, hyperphosphorylation of MAP2, like its homolog MAPT in dementia pathogenesis, may mediate impairments of neuronal structure and function downstream of many different genetic (and possibly environmental) risk factors. The potential impact of this conceptualization is that it identifies a bottleneck of molecular pathology providing a narrow set of targets for prevention and treatment for a large proportion of individuals with schizophrenia, regardless of the polygenic origins of their illness. Identification of the specific binding partners of MAP2 within the protein translational machinery, e.g. via approaches such as chemical cross-linking,[80] may provide leads to small molecules or peptides that disrupt this interaction and could then be tested as novel therapies for these individuals.

1. Kavanagh DH, Tansey KE, O'Donovan MC, Owen MJ. Schizophrenia genetics: emerging themes for a complex disorder. *Mol Psychiatry.* 2015;20(1):72-76.
2. Moyer CE, Shelton MA, Sweet RA. Dendritic spine alterations in schizophrenia. *Neurosci Lett.* 2014.
3. Lewis DA, Lieberman JA. Catching up on schizophrenia: natural history and neurobiology. *Neuron.* 2000;28(2):325-334.
4. Hegarty JD, Baldessarini RJ, Tohen M, Waternaux C, Oepen G. One hundred years of schizophrenia: a meta-analysis of the outcome literature. *Am J Psychiatry.* 1994;151(10):1409-1416.
5. Arnold SE, Lee VM, Gur RE, Trojanowski JQ. Abnormal expression of two microtubule-associated proteins (MAP2 and MAP5) in specific subfields of the hippocampal formation in schizophrenia. *Proc Natl Acad Sci U S A.* 1991;88(23):10850-10854.
6. Jones LB, Johnson N, Byne W. Alterations in MAP2 immunocytochemistry in areas 9 and 32 of schizophrenic prefrontal cortex. *Psychiatry Res.* 2002;114(3):137-148.
7. Rioux L, Ruscheinsky D, Arnold SE. Microtubule-associated protein MAP2 expression in olfactory bulb in schizophrenia. *Psychiatry Res.* 2004;128(1):1-7.
8. Rosoklija G, Keilp JG, Toomayan G, et al. Altered subicular MAP2 immunoreactivity in schizophrenia. *Prilozi.* 2005;26(2):13-34.
9. Somenarain L, Jones LB. A comparative study of MAP2 immunostaining in areas 9 and 17 in schizophrenia and Huntington chorea. *J Psychiatr Res.* 2010;44(11):694-699.
10. Shelton MA, Newman JT, Gu H, et al. Loss of Microtubule-Associated Protein 2 Immunoreactivity Linked to Dendritic Spine Loss in Schizophrenia. *Biol Psychiatry.* 2015;78(6):374-385.
11. Marchisella F, Coffey ET, Hollos P. Microtubule and microtubule associated protein anomalies in psychiatric disease. *Cytoskeleton (Hoboken).* 2016;73(10):596-611.

12. McKinney BC, MacDonald ML, Newman JT, et al. Density of small dendritic spines and microtubule-associated-protein-2 immunoreactivity in the primary auditory cortex of subjects with schizophrenia. *Neuropsychopharmacology.* 2019;44(6):1055-1061.
13. Arnold SE, Lee VM, Gur RE, Trojanowski JQ. Abnormal expression of two microtubule-associated proteins (MAP2 and MAP5) in specific subfields of the hippocampal formation in schizophrenia. *Proc Natl Acad Sci U S A.* 1991;88(23):10850-10854.
14. Sanchez C, Diaz-Nido J, Avila J. Phosphorylation of microtubule-associated protein 2 (MAP2) and its relevance for the regulation of the neuronal cytoskeleton function. *Prog Neurobiol.* 2000;61(2):133-168.
15. Halpain S, Greengard P. Activation of NMDA receptors induces rapid dephosphorylation of the cytoskeletal protein MAP2. *Neuron.* 1990;5(3):237-246.
16. Quinlan EM, Halpain S. Postsynaptic mechanisms for bidirectional control of MAP2 phosphorylation by glutamate receptors. *Neuron.* 1996;16(2):357-368.
17. Quinlan EM, Halpain S. Emergence of activity-dependent, bidirectional control of microtubule-associated protein MAP2 phosphorylation during postnatal development. *J Neurosci.* 1996;16(23):7627-7637.
18. Davare MA, Dong F, Rubin CS, Hell JW. The A-kinase anchor protein MAP2B and cAMP-dependent protein kinase are associated with class C L-type calcium channels in neurons. *J Biol Chem.* 1999;274(42):30280-30287.
19. Hoshi M, Ohta K, Gotoh Y, et al. Mitogen-activated-protein-kinase-catalyzed phosphorylation of microtubule-associated proteins, microtubule-associated protein 2 and microtubule-associated protein 4, induces an alteration in their function. *Eur J Biochem.* 1992;203(1-2):43-52.
20. Biological insights from 108 schizophrenia-associated genetic loci. *Nature.* 2014;511(7510):421-427.
21. Purcell SM, Moran JL, Fromer M, et al. A polygenic burden of rare disruptive mutations in schizophrenia. *Nature.* 2014;506(7487):185-190.
22. Salvoro C, Bortoluzzi S, Coppe A, et al. Rare Risk Variants Identification by Identity-by-Descent Mapping and Whole-Exome Sequencing Implicates Neuronal Development Pathways in Schizophrenia and Bipolar Disorder. *Mol Neurobiol.* 2018.
23. Gusev A, Mancuso N, Won H, et al. Transcriptome-wide association study of schizophrenia and chromatin activity yields mechanistic disease insights. *Nat Genet.* 2018;50(4):538-548.
24. Mohan R, John A. Microtubule-associated proteins as direct crosslinkers of actin filaments and microtubules. *IUBMB Life.* 2015;67(6):395-403.
25. Sweet RA, Bergen SE, Sun Z, Sampson AR, Pierri JN, Lewis DA. Pyramidal cell size reduction in schizophrenia: evidence for involvement of auditory feedforward circuits. *Biol Psychiatry.* 2004;55(12):1128-1137.
26. Pierri JN, Volk CL, Auh S, Sampson A, Lewis DA. Decreased somal size of deep layer 3 pyramidal neurons in the prefrontal cortex of subjects with schizophrenia. *Arch Gen Psychiatry.* 2001;58(5):466-473.
27. Sweet RA, Pierri JN, Auh S, Sampson AR, Lewis DA. Reduced pyramidal cell somal volume in auditory association cortex of subjects with schizophrenia. *Neuropsychopharmacology.* 2003;28(3):599-609.
28. Rajkowska G, Selemon LD, Goldman-Rakic PS. Neuronal and glial somal size in the prefrontal cortex: a postmortem morphometric study of schizophrenia and Huntington disease. *Archives of General Psychiatry.* 1998;55:215-224.
29. Black JE, Kodish IM, Grossman AW, et al. Pathology of layer V pyramidal neurons in the prefrontal cortex of patients with schizophrenia. *American Journal of Psychiatry.* 2004;161(4):742-744.
30. Broadbelt K, Byne W, Jones LB. Evidence for a decrease in basilar dendrites of pyramidal cells in schizophrenic medial prefrontal cortex. *Schizophr Res.* 2002;58(1):75-81.
31. Glantz LA, Lewis DA. Decreased dendritic spine density on prefrontal cortical pyramidal neurons in schizophrenia. *Archives of General Psychiatry.* 2000;57:65-73.
32. Konopaske GT, Lange N, Coyle JT, Benes FM. Prefrontal Cortical Dendritic Spine Pathology in Schizophrenia and Bipolar Disorder. *JAMA Psychiatry.* 2014.
33. Kalus P, Müller TJ, Zuschratter W, Senitz D. The dendritic architecture of prefrontal pyramidal neurons in schizophrenic patients. *Neuroreport.* 2000;11(16):3621-3625.
34. Garey LJ, Ong WY, Patel TS, et al. Reduced dendritic spine density on cerebral cortical pyramidal neurons in schizophrenia. *Journal of Neurology, Neurosurgery and Psychiatry.* 1998;65:446-453.
35. Rosoklija G, Toomayan G, Ellis SP, et al. Structural abnormalities of subicular dendrites in subjects with schizophrenia and mood disorders. *Archives of General Psychiatry.* 2000;57:349-356.

36. Sweet RA, Henteleff RA, Zhang W, Sampson AR, Lewis DA. Reduced dendritic spine density in auditory cortex of subjects with schizophrenia. *Neuropsychopharmacology.* 2009;34(2):374-389.
37. McKinney BC, MacDonald ML, Newman JT, et al. Density of small dendritic spines and microtubule-associated-protein-2 immunoreactivity in the primary auditory cortex of subjects with schizophrenia. *Neuropsychopharmacology.* 2019.
38. Braganza A, Li J, Zeng X, et al. UBE3B is a calmodulin-regulated, mitochondrion-associated E3 ubiquitin ligase. *Journal of Biological Chemistry.* 2017;292(6):2470-2484.
39. Glantz LA, Lewis DA. Decreased dendritic spine density on prefrontal cortical pyramidal neurons in schizophrenia. *Arch Gen Psychiatry.* 2000;57(1):65-73.
40. Sweet RA, Henteleff RA, Zhang W, Sampson AR, Lewis DA. Reduced dendritic spine density in auditory cortex of subjects with schizophrenia. *Neuropsychopharmacology.* 2009;34(2):374-389.
41. Shelton MA, Newman JT, Gu H, et al. Loss of Microtubule-Associated Protein 2 Immunoreactivity Linked to Dendritic Spine Loss in Schizophrenia. *Biol Psychiatry.* 2015;78(6):374-385.
42. Deo AJ, Cahill ME, Li S, et al. Increased expression of Kalirin-9 in the auditory cortex of schizophrenia subjects: Its role in dendritic pathology. *Neurobiology of disease.* 2011(Journal Article).
43. O'Connor JA, Hasenkamp W, Horman BM, Muly EC, Hemby SE. Region specific regulation of NR1 in rhesus monkeys following chronic antipsychotic drug administration. *Biol Psychiatry.* 2006;60(6):659-662.
44. O'Connor JA, Muly EC, Arnold SE, Hemby SE. AMPA receptor subunit and splice variant expression in the DLPFC of schizophrenic subjects and rhesus monkeys chronically administered antipsychotic drugs. *Schizophr Res.* 2007;90(1-3):28-40.
45. MacDonald ML, Ding Y, Newman J, et al. Altered glutamate protein co-expression network topology linked to spine loss in the auditory cortex of schizophrenia. *Biol Psychiatry.* 2015;77(11):959-968.
46. MacLean B, Tomazela DM, Shulman N, et al. Skyline: an open source document editor for creating and analyzing targeted proteomics experiments. *Bioinformatics.* 2010;26(7):966-968.
47. Schilling B, Rardin MJ, MacLean BX, et al. Platform-independent and label-free quantitation of proteomic data using MS1 extracted ion chromatograms in Skyline application to protein acetylation and phosphorylation. *Molecular & Cellular Proteomics.* 2012;11(5):202-214.
48. Schmidt EK, Clavarino G, Ceppi M, Pierre P. SUnSET, a nonradioactive method to monitor protein synthesis. *Nat Methods.* 2009;6(4):275-277.
49. Langfelder P, Horvath S. WGCNA: an R package for weighted correlation network analysis. *BMC Bioinformatics.* 2008;9:559.
50. MacDonald M GM, Newman J, Sun Z, Kannarkat J, Salisbury R, Glausier J, Ding Y, Lewis DA, Yates N, Sweet RA. Synaptic Proteome Alterations in the Primary Auditory Cortex of Schizophrenia. *bioRxiv.* 2019.
51. Glausier JR, Kelly MA, Salem S, Chen K, Lewis DA. Proxy measures of premortem cognitive aptitude in postmortem subjects with schizophrenia. *Psychol Med.* 2019:1-8.
52. Regan P, Piers T, Yi JH, et al. Tau phosphorylation at serine 396 residue is required for hippocampal LTD. *J Neurosci.* 2015;35(12):4804-4812.
53. Xia D, Li C, Gotz J. Pseudophosphorylation of Tau at distinct epitopes or the presence of the P301L mutation targets the microtubule-associated protein Tau to dendritic spines. *Biochim Biophys Acta.* 2015;1852(5):913-924.
54. Bramblett GT, Goedert M, Jakes R, Merrick SE, Trojanowski JQ, Lee VM. Abnormal tau phosphorylation at Ser396 in Alzheimer's disease recapitulates development and contributes to reduced microtubule binding. *Neuron.* 1993;10(6):1089-1099.
55. Mondragon-Rodriguez S, Perry G, Luna-Munoz J, Acevedo-Aquino MC, Williams S. Phosphorylation of tau protein at sites Ser(396-404) is one of the earliest events in Alzheimer's disease and Down syndrome. *Neuropathol Appl Neurobiol.* 2014;40(2):121-135.
56. Jansen S, Melkova K, Trosanova Z, et al. Quantitative mapping of microtubule-associated protein 2c (MAP2c) phosphorylation and regulatory protein 14-3-3zeta-binding sites reveals key differences between MAP2c and its homolog Tau. *J Biol Chem.* 2017;292(16):6715-6727.
57. Novacek J, Janda L, Dopitova R, Zidek L, Sklenar V. Efficient protocol for backbone and side-chain assignments of large, intrinsically disordered proteins: transient secondary structure analysis of 49.2 kDa microtubule associated protein 2c. *J Biomol NMR.* 2013;56(4):291-301.

58. Lippens G, Landrieu I, Smet C, et al. NMR Meets Tau: Insights into Its Function and Pathology. *Biomolecules.* 2016;6(2).
59. Sillen A, Barbier P, Landrieu I, et al. NMR investigation of the interaction between the neuronal protein tau and the microtubules. *Biochemistry.* 2007;46(11):3055-3064.
60. Schwalbe M, Kadavath H, Biernat J, et al. Structural Impact of Tau Phosphorylation at Threonine 231. *Structure.* 2015;23(8):1448-1458.
61. Lyons AJ, Gandhi NS, Mancera RL. Molecular dynamics simulation of the phosphorylation-induced conformational changes of a tau peptide fragment. *Proteins.* 2014;82(9):1907-1923.
62. Amniai L, Lippens G, Landrieu I. Characterization of the AT180 epitope of phosphorylated Tau protein by a combined nuclear magnetic resonance and fluorescence spectroscopy approach. *Biochem Biophys Res Commun.* 2011;412(4):743-746.
63. Sibille N, Huvent I, Fauquant C, et al. Structural characterization by nuclear magnetic resonance of the impact of phosphorylation in the proline-rich region of the disordered Tau protein. *Proteins.* 2012;80(2):454-462.
64. Mukrasch MD, von Bergen M, Biernat J, et al. The "jaws" of the tau-microtubule interaction. *J Biol Chem.* 2007;282(16):12230-12239.
65. Gustke N, Trinczek B, Biernat J, Mandelkow EM, Mandelkow E. Domains of tau protein and interactions with microtubules. *Biochemistry.* 1994;33(32):9511-9522.
66. Kadavath H, Jaremko M, Jaremko L, Biernat J, Mandelkow E, Zweckstetter M. Folding of the Tau Protein on Microtubules. *Angew Chem Int Ed Engl.* 2015;54(35):10347-10351.
67. Harindranath K, Yunior CF, Mariusz J, et al. The Binding Mode of a Tau Peptide with Tubulin. *Angewandte Chemie International Edition.* 2018;57(12):3246-3250.
68. Kapitein LC, Yau KW, Gouveia SM, et al. NMDA receptor activation suppresses microtubule growth and spine entry. *J Neurosci.* 2011;31(22):8194-8209.
69. Gumy LF, Katrukha EA, Grigoriev I, et al. MAP2 Defines a Pre-axonal Filtering Zone to Regulate KIF1- versus KIF5-Dependent Cargo Transport in Sensory Neurons. *Neuron.* 2017;94(2):347-362 e347.
70. Farah CA, Liazoghli D, Perreault S, et al. Interaction of microtubule-associated protein-2 and p63: a new link between microtubules and rough endoplasmic reticulum membranes in neurons. *J Biol Chem.* 2005;280(10):9439-9449.
71. Huang dW, Sherman BT, Lempicki RA. Systematic and integrative analysis of large gene lists using DAVID bioinformatics resources. *Nat Protoc.* 2009;4(1):44-57.
72. Johnson GV, Jope RS. The role of microtubule-associated protein 2 (MAP-2) in neuronal growth, plasticity, and degeneration. *J Neurosci Res.* 1992;33(4):505-512.
73. Itoh TJ, Hisanaga S, Hosoi T, Kishimoto T, Hotani H. Phosphorylation states of microtubule-associated protein 2 (MAP2) determine the regulatory role of MAP2 in microtubule dynamics. *Biochemistry.* 1997;36(41):12574-12582.
74. Evans DB, Rank KB, Bhattacharya K, Thomsen DR, Gurney ME, Sharma SK. Tau phosphorylation at serine 396 and serine 404 by human recombinant tau protein kinase II inhibits tau's ability to promote microtubule assembly. *J Biol Chem.* 2000;275(32):24977-24983.
75. Lim RW, Halpain S. Regulated association of microtubule-associated protein 2 (MAP2) with Src and Grb2: evidence for MAP2 as a scaffolding protein. *J Biol Chem.* 2000;275(27):20578-20587.
76. Hanus C, Schuman EM. Proteostasis in complex dendrites. *Nature Reviews Neuroscience.* 2013;14(9):638.
77. Buxbaum AR, Haimovich G, Singer RH. In the right place at the right time: visualizing and understanding mRNA localization. *Nature reviews Molecular cell biology.* 2015;16(2):95.
78. Kovács T, Kelemen O, Kéri S. Decreased fragile X mental retardation protein (FMRP) is associated with lower IQ and earlier illness onset in patients with schizophrenia. *Psychiatry research.* 2013;210(3):690-693.
79. Pasciuto E, Bagni C. SnapShot: FMRP mRNA targets and diseases. *Cell.* 2014;158(6):1446-1446 e1441.
80. Shi Y, Pellarin R, Fridy PC, et al. A strategy for dissecting the architectures of native macromolecular assemblies. *Nature methods.* 2015;12(12):1135.

Fig 2. WGCNA analysis of MAP2 phosphopeptides. (A) Three distinct modules (blue, brown, and turquoise, were identified. (B) Network diagram of phosphopeptide modules. Arrow indicates S1782. Node size is proportional to connectivity, line thickness is proportional to correlation. (C) Modules shown on MAP2B sequence. Arrow indicates S1782. (D) pS1782 negatively correlates with dendritic spine density.

NPC = nonpsychiatric control, Sz subjects grouped by MAP2 immunoreactivity as either normal (MAP2-IR_{NL}) or low (MAP2-IR_{LOW})

Fig 3. Computational modeling of MAP2 pS1782 alters predicted structure and reduces microtubule binding. (A) Snapshot of the C-terminal domain of MAP2. Amino acids A1776 to Q1781 form an extended β strand (red β strand) that is occluded by an opposing β strand. In much of the non-phosphorylated ensemble, there is found to be helical propensity in or near regions S1759 to R1765 (yellow) which is not found in the phosphorylated ensembles. In pMAP2 (pS1782) the β strand at A1776 to Q1781 is no longer occluded by another β strand; this is predicted to reduce microtubule binding and enhance interactions with other proteins. The effect of phosphorylation is recapitulated by phosphomimetic mutation S1782E (data not shown). (B) Reduced MT-binding in MAP2c with the phosphomimetic mutation S426E, homologous to S1782 in full length MAP2b relative to MAP2c-WT. 30µL of cell lysate from transiently transfected HEK cells was subjected to *in vitro* MT-binding assay and supernatant (S) and pellet (P) fractions were subjected to SDS-PAGE. (C) Densitometric analysis of gels shows decreased MT binding in the S426E mutant compared to WT. Data shown are from 3 independent experiments, ± SEM. *$p < 0.05$

Figure 4. Co-IP of MAP2 from mouse brain and functional effects of S1782E on protein synthesis. (A) Agarose gel image confirming degradation of RNA in tissue lysate prior to co-IP. (B) MAP2c was IP'd from RNAse treated mouse brain cortical homogenate (sup = supernatant, IP = immunoprecipitant). Beads without antibody coupling were used as a control. Individual channels are shown vertically (MAP2 in 800 channel, β-tubulin in 700 channel). (C) Using conservative cutoff criteria of q<.05, 6095 peptides (red) from 590 proteins were identified as potential MAP2 interactors. (D) Puromycin incorporation was detected via western blotting following a 1h treatment of transiently transfected HEK293 cells expressing MAP2c-WT or MAP2c-S426E for 48h. (E) Densitometric quantification of relative puromycin incorporation normalized to MAP2 expression levels. N=4, data shown are average across experiments ± SEM. *$p < 0.1$, **p<.05.

Protein Name	Module	Peptide Modified Sequence	Starting AA number	FoldChange (MAP2-IR$_{LOW}$ SZ vs Ctrl)	p value	q value	FoldChange (MAP-IR$_{NL}$ SZ vs Ctrl)	p value	q value	FoldChange (All SZ vs Ctrl)	p value	q value
MTAP2_HUMAN	Blue	ADEGKKE*T[+80]S[+80]*PESSLIQDEIAVK	1147	1.236	0.22470	0.31113	1.393	0.16049	0.32098	0.35948157	0.1072774	0.1609162
MTAP2_HUMAN	Blue	SGTSTPTTPGSTAITPG*T[+80]*PP*S[+80]Y[+80]*SSR	1588	7.293	0.00001	0.00019	3.064	0.03217	0.20111	2.47771553	2.104E-05	0.0003788
MTAP2_HUMAN	Blue	VAIIR*T[+80]*PPK*S[+80]*PA*T[+80]*PK	1644	1.782	0.01940	0.04364	1.657	0.11801	0.27978	0.80084395	0.0107894	0.030062
MTAP2_HUMAN	Blue	VAIIRT[+80]PPKS[+80]PATPK	1644	1.665	0.40104	0.48125	4.401	0.07646	0.22938	1.17111812	0.1395419	0.179411
MTAP2_HUMAN	Blue	ARVDHGAEIITQS[+80]PGR	1772	5.947	0.00147	0.00663	2.452	0.19721	0.35498	2.17498811	0.0024017	0.0144102
MTAP2_HUMAN	Blue	VDHGAEIITQS[+80]PGR	1774	8.791	0.00018	0.00162	4.060	0.04749	0.20111	2.78965661	0.0001733	0.0015597
MTAP2_HUMAN	Blue	RL*S[+80]*NVS*S[+80]*SG*S[+80]*INLLESPQLATLAEDVTAALAK	1792	0.141	0.00064	0.00385	0.617	0.48590	0.58308	-2.16377574	0.0037738	0.0169822
MTAP2_HUMAN	Brown	ESQP*S[+80]*PPAQEAG*Y[+80]*S*T[+80]*LAQSYPSDLPEEPSSPQER	625	0.638	0.01021	0.03675	1.002	0.99259	0.99310	-0.44607367	0.0506318	0.0828521
MTAP2_HUMAN	Brown	DGS[+80]PEAPASPEREEVALSEYK	1344	0.794	0.12603	0.20623	0.886	0.54275	0.61059	-0.47145828	0.0171191	0.0342382
MTAP2_HUMAN	Brown	DGSPEAPAS[+80]PEREEVALSEYK	1344	0.687	0.01610	0.04141	0.803	0.27391	0.43783	-0.28368005	0.1365374	0.179411
MTAP2_HUMAN	Turquoise	DQTAALPLAAEETANLPP*S[+80*]PPPS*S[+80]*PASEQT*T[+80]*VTVEEDLLTASK	118	0.921	0.66940	0.75308	1.293	0.32429	0.44902	0.03361841	0.8922331	0.9250379
MTAP2_HUMAN	Turquoise	ESQPSPPAQEAGYSTLAQSYPSDLPEEPSS[+80]PQER	625	1.795	0.04746	0.08543	2.571	0.01925	0.20111	1.00482271	0.0093543	0.030062
MTAP2_HUMAN	Turquoise	RKS[+80]VPSETVVEDSR	829	0.556	0.32844	0.42228	1.971	0.40090	0.51545	-0.27993877	0.7200388	0.8100437
MTAP2_HUMAN	Turquoise	KE*T[+80]S[+80]*PE*S[+80]S[+80]*LIQDEIAVK	1152	1.350	0.04485	0.08543	1.527	0.03613	0.20111	0.48787546	0.0116908	0.030062
MTAP2_HUMAN	Turquoise	E*T[+80]S[+80]*PE*S[+80]S[+80]*LIQDEIAVK	1153	1.314	0.15557	0.23336	1.653	0.05586	0.20111	0.49653156	0.046599	0.0828521
MTAP2_HUMAN	Turquoise	DGS[+80]PEAPAS[+80]PEREEVALSEYK	1344	0.941	0.80149	0.84863	1.668	0.12435	0.27978	0.16900296	0.5977232	0.7172678
MTAP2_HUMAN	Turquoise	VSDGVTKS[+80]PEKR	1527	0.953	0.90921	0.90921	0.995	0.99310	0.99310	-0.0501051	0.9250379	0.9250379
MTAP2_HUMAN	Turquoise	VAIIRT[+80]PPK	1644	2.455	0.01234	0.03703	1.624	0.29189	0.43783	1.11067672	0.0148646	0.0334454

Module	Starting Amino Acid # for Included Phosphopeptides	Correlation With Dendritic Spine Density	Signficant Correlations with Synaptic Protein Levels N (% R < 0)	Correlation With Subject SES
Blue	1147, 1588, 1644, 1644, 1769, 1774, 1792	R = -0.56 P = 0.001	57 (88%)	R = -0.47 P = 0.01
Brown	625, 1344, 1344	R = 0.44 P = 0.01	10 (40%)	R = 0.50 P = 0.007
Turquoise	118, 625, 831, 1152, 1153, 1344, 1527, 1644	R = 0.10 P = 0.57	0 (N/A)	R = 0.22 P = 0.26

A.

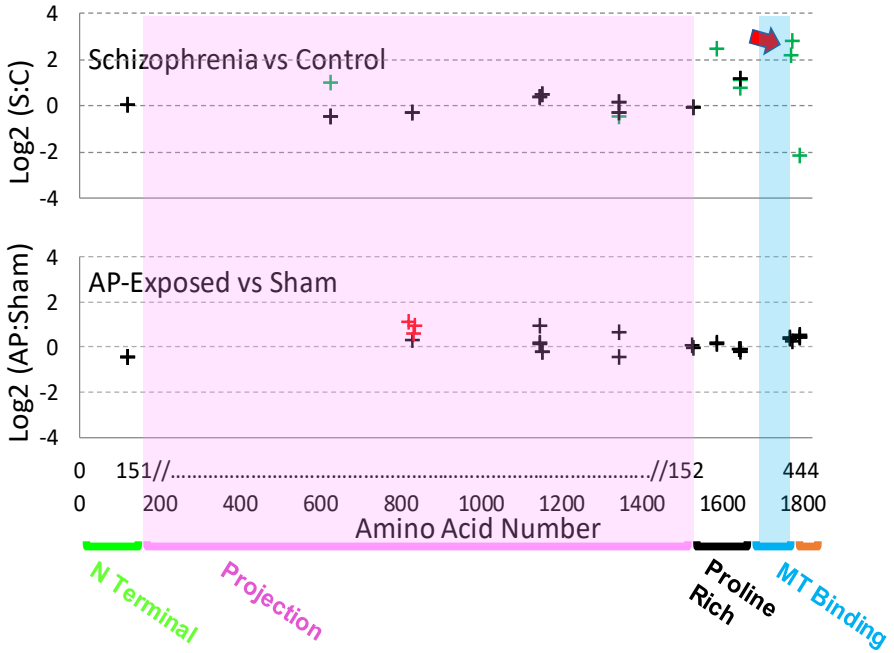

B.

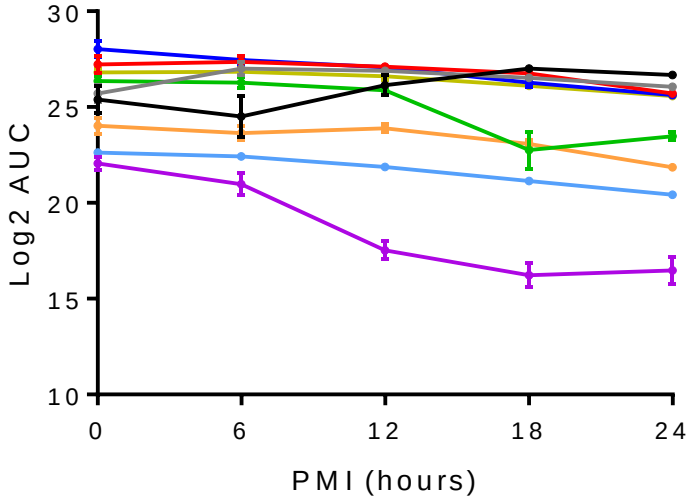

DGS[+80]PEAPAS[+80]PEREEVALSEYK

DGS[+80]PEAPASPEREEVALSEYK

DQTAALPLAAEETANLPP*S[+80]*PPPS*S[+80]*PASEQT*T[+80]*VTVEEDLLTASK

E*T[+80]S[+80]*PE*S[+80]S[+80]*LIQDEIAVK

RL*S[+80]*NVS*S[+80]*SG*S[+80]*INLLESPQLATLAEDVTAALAK

SGTSTPTTPGSTAITPG*T[+80]*PP*S[+80]Y[+80]*SSR

VAIIR*T[+80]*PPK*S[+80]*PA*T[+80]*PK

VDHGAEIITQS[+80]PGR

VSDGVTKS[+80]PEKR

A.

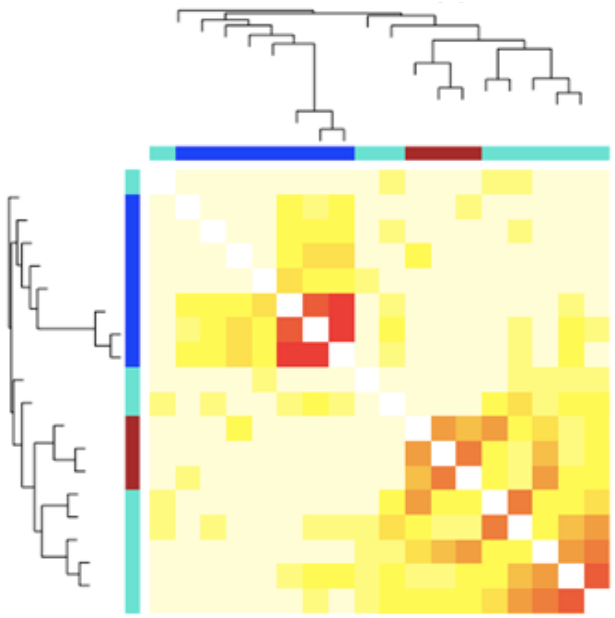

B.

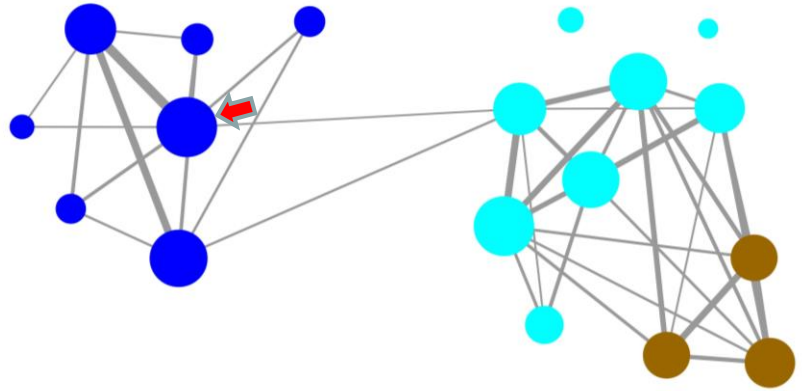

C.

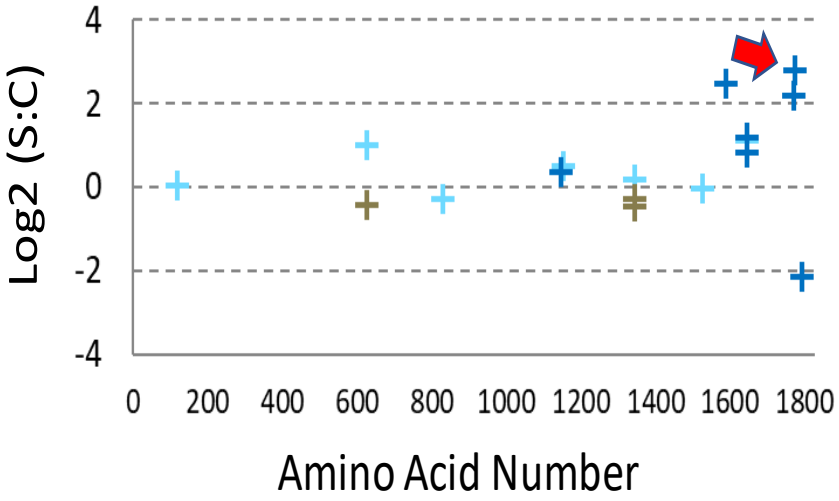
Log2 (S:C)
4
2
0
-2
-4
0
200
400
600
800
1000
1200
1400
1600
1800
Amino Acid Number

D.

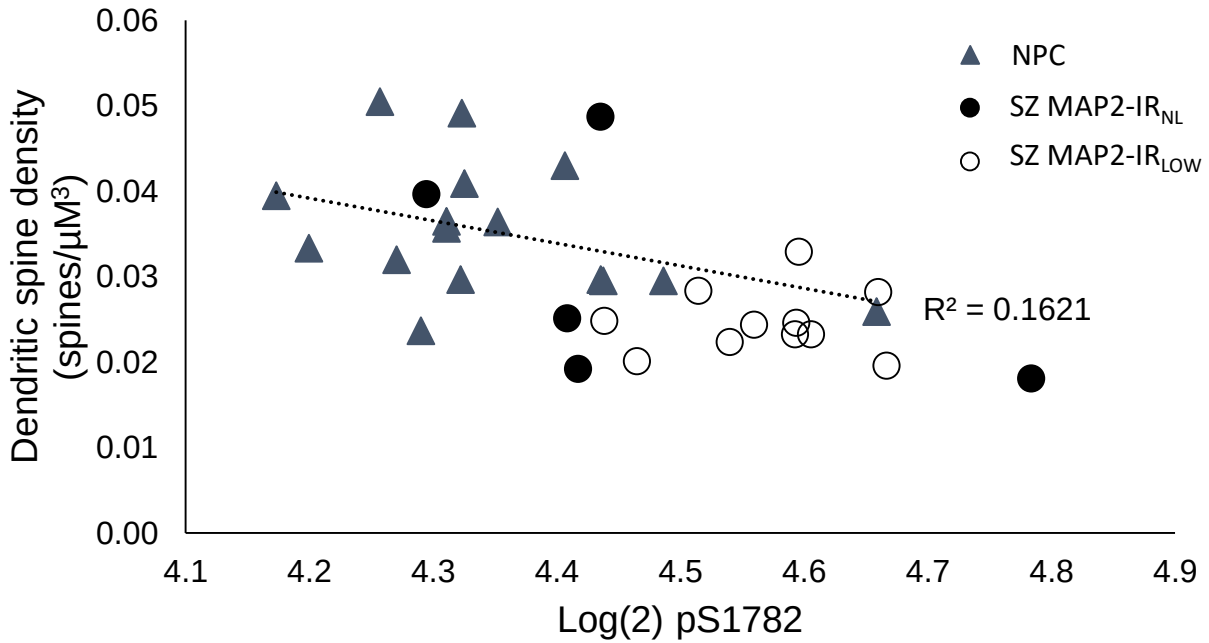
Dendritic spine density (spines/µM³)
0.06
0.05
0.04
0.03
0.02
0.01
0.00
4.1
4.2
4.3
4.4
4.5
4.6
4.7
4.8
4.9
Log(2) pS1782
NPC
SZ MAP2-IR$_{NL}$
SZ MAP2-IR$_{LOW}$
R² = 0.1621

A.

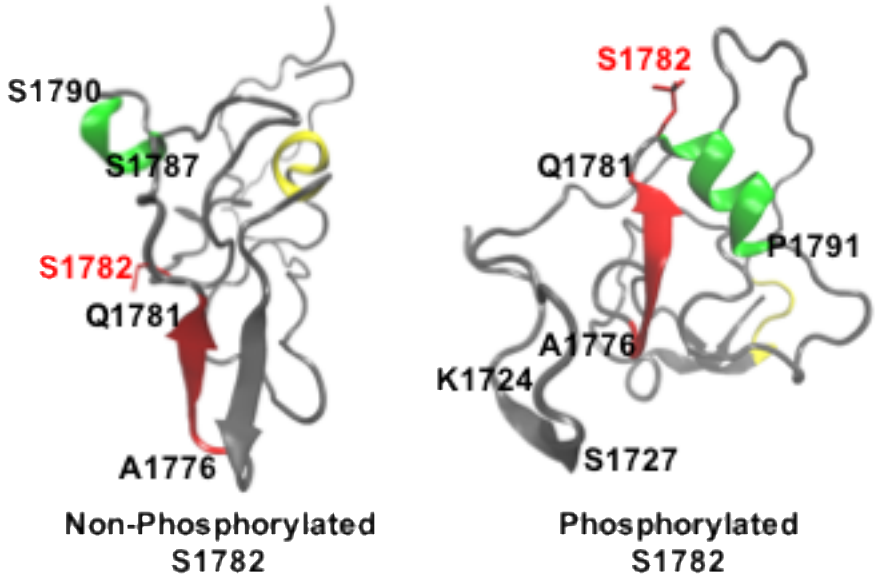
S1790
S1787
S1782
Q1781
A1776
Non-Phosphorylated
S1782
S1782
Q1781
P1791
A1776
K1724
S1727
Phosphorylated
S1782

B.

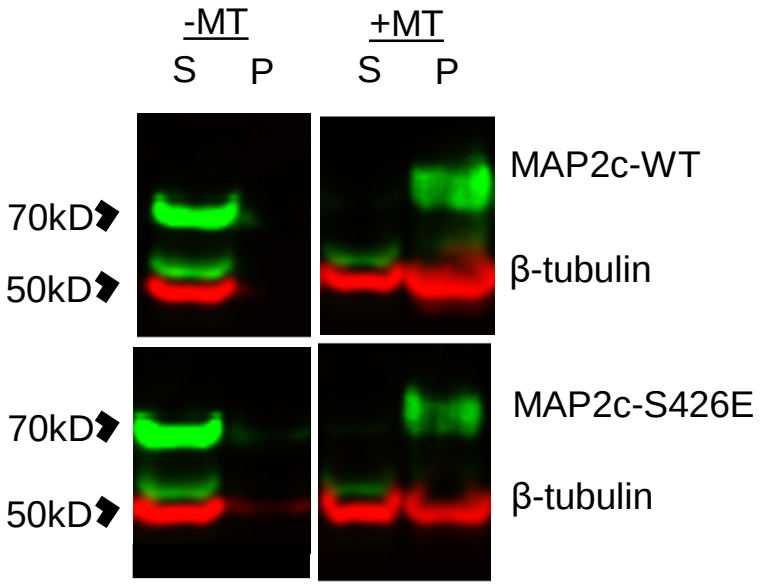
-MT
+MT
S
P
S
P
70kD
50kD
MAP2c-WT
β-tubulin
70kD
50kD
MAP2c-S426E
β-tubulin

C.

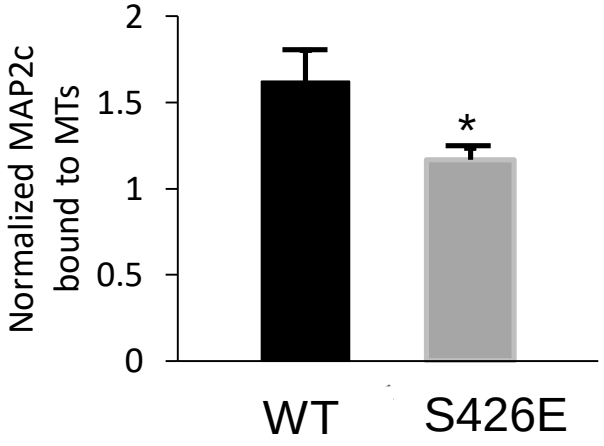
Normalized MAP2c bound to MTs
2
1.5
1
0.5
0
*
WT
S426E

A.

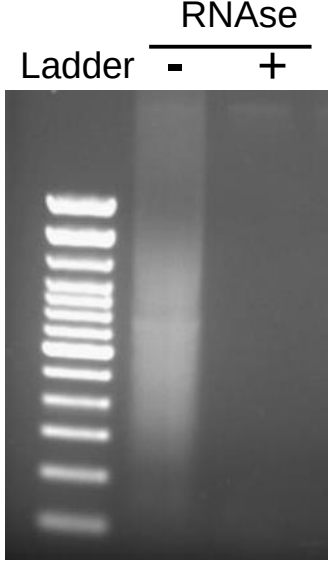
RNAse
Ladder
-
+

B.

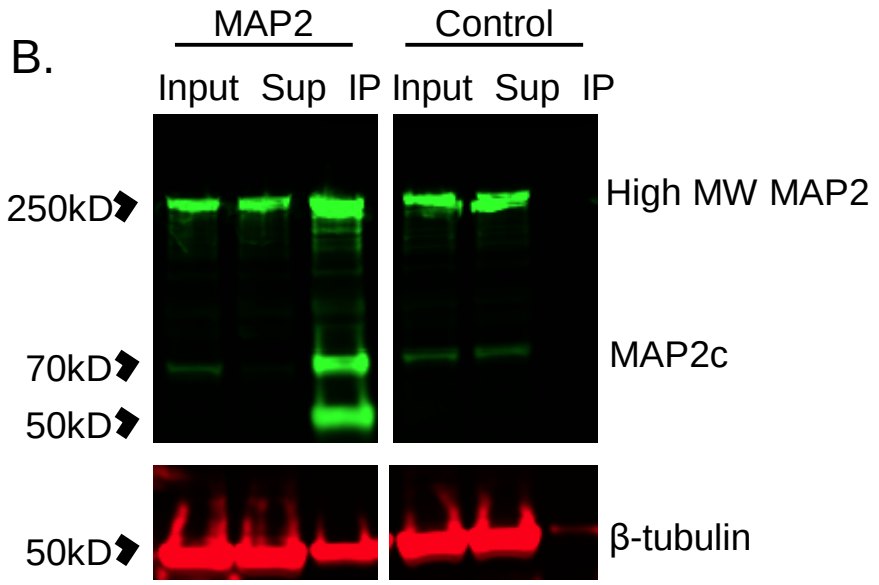
MAP2
Control
Input
Sup
IP
Input
Sup
IP
250kD
70kD
50kD
50kD
High MW MAP2
MAP2c
β-tubulin

C.

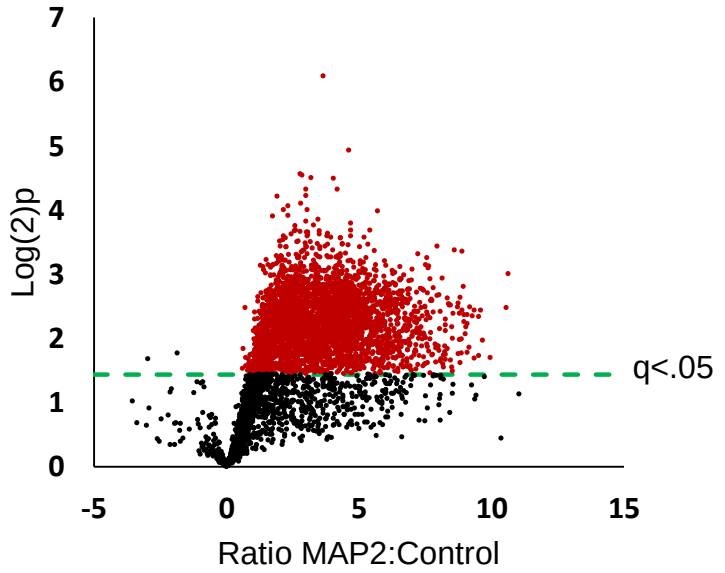
Log(2)p
7
6
5
4
3
2
1
0
-5
0
5
10
15
q<.05
Ratio MAP2:Control

D.

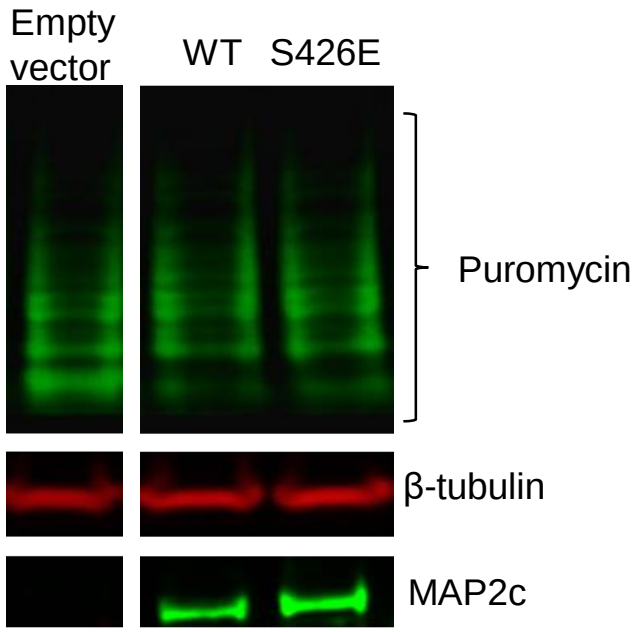
Empty vector
WT
S426E
Puromycin
β-tubulin
MAP2c

E.

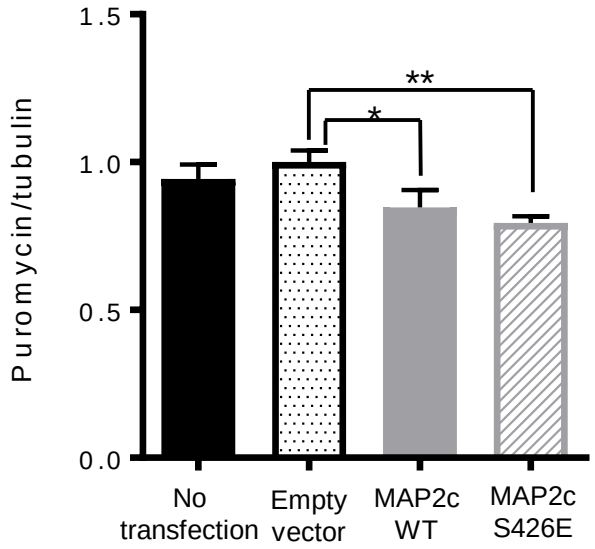
Puromycin/tubulin
1.5
1.0
0.5
0.0
**
*
No transfection
Empty vector
MAP2c WT
MAP2c S426E